Int. J. Heat Mass Transfer. Vol. 35, No. 11, pp. 2837–2847, 1992
Printed in Great Britain

0017–9310/92 $5.00+0.00

Heat transfer and convection characteristics of a superheated turbulent jet interacting with a solid object

WEI SHYY,† YUAN PANG,‡ MING-HSIUNG CHEN† and DANIEL Y. WEI‡

†Department of Aerospace Engineering, Mechanics and Engineering Science, University of Florida, Gainesville, FL 32611, U.S.A.

‡GE Aircraft Engines, Engineering Materials Technology Laboratories, Lynn, MA 01910, U.S.A.

(*Received* 14 *June* 1991 *and in final form* 10 *December* 1991)

Abstract—The present study attempts to investigate numerically the heat transfer and associated convection characteristics arising from the interaction between a superheated turbulent argon jet and a solid object, a topic of critical importance to the modern rapid solidification processes. Two flow configurations are simulated, one a planar case that includes a slot jet issued into a circular cylindrical chamber and impinged on a solid cylinder, and the other an axisymmetric case that includes a circular jet issued into a circular cylindrical chamber and impinged on a solid sphere. The effects of the turbulence intensity of the incoming jet on the convection and heat transfer characteristics are studied; in both configurations the turbulent transport can help enhance the heat transfer rate, causing highly non-uniform Nusselt number distributions around the object. Furthermore, due to the differences caused by the two geometries, flow separation can be completely suppressed by high turbulence intensity in the planar configuration, but not in the axisymmetric configuration. Efforts are made to interpret and elucidate the various characteristics exhibited by the solutions obtained, and to gain physical insights of the relevant processing conditions.

1. INTRODUCTION

THROUGHOUT metallurgical processing, quenching treatments have had an important role in the production and control of alloy microstructures. In order to attain a satisfactory fineness of the materials, high cooling rates during solidification are usually required. In this regard, in the 1930s, gas atomization came into play for the commercial production of metal powders. In the 1950s, the concept of rapid cooling began to be applied deliberately to ingots for improving their workability and to castings for enhancing their properties. Since then, the area of rapid solidification processing (RSP) has been experiencing fast growth and high visibility [1–3]. A review of the existing literature shows that while significant advances have been made in the engineering aspects of rapid solidification, the understanding and capability of predicting the process dynamics is still far from satisfactory. For example, the determination of the heat transfer coefficient, h, in a realistic operating environment is not easy. Estimation, usually empirically based, of this parameter often contains large uncertainty; for many processes, the values of h yielded by different formulas can vary by more than an order of magnitude [1, p. 23].

Although the two-phase flow and solidification characteristics are obviously critical to the success of the RSP, their behaviors are affected by the initial heating treatment of the solid object by a single phase jet. For many practical RSP applications, the process usually starts by issuing a high temperature jet without solid particles to heat up the solid object as well as the environment within the enclosure. The thermal characteristics on the surface of the solid object in terms of temperature and temperature gradient distribution can substantially affect the subsequent operation of RSP itself, dictating the time scale of solidification and the microstructure of the solidified materials.

The present work attempts to address the issue of the heat transfer and related transport characteristics during the initial heat-up process based on detailed numerical modeling. The physical problem under study here is that of a solid object opposing a fast moving and superheated fluid stream, and the heat is withdrawn through the solid. The flow conditions investigated are those of a high temperature, high speed jet (7000 K and 100 m s^{-1} at the inlet) issued into a chamber and impinged on a solid object of a constant wall temperature of 1000 K. In order to investigate the characteristics associated with the turbulent transport processes under different operating conditions, two cases including a 2-D planar configuration, which contains a slot jet interacting with a solid circular cylinder, and a 2-D axisymmetric configuration, which contains a round jet impinging on a solid sphere, are modeled.

The goals of the present study are to elucidate the convective characteristics caused by jet/solid interaction, to determine the distribution of heat transfer coefficient and the Nusselt number, and to investigate the effect of turbulence on the overall effectiveness of the cooling and mixing mechanisms of the incoming jet, an issue critical to RSP. Care has been taken in

mapping the geometric variation by a non-orthogonal coordinate system, and in improving the spatial resolution by utilizing an adaptive grid technique. A k–ε two-equation model aided by the low Reynolds number modification is adopted as the turbulence closure. In the present study, only the single-phase flow of argon gas is considered in order to establish the basic physical picture of RSP. As already noted, the single-phase heat transfer process often plays a very critical role in determining the quality of an RSP operation since many aspects of the overall thermal characteristics of the system are dictated by it. It is this aspect of RSP that will be focused on in the present work. Other issues such as multiphase flow, solidification kinetics, turbulence modulation and radiation due to particle loading effects will not be addressed here.

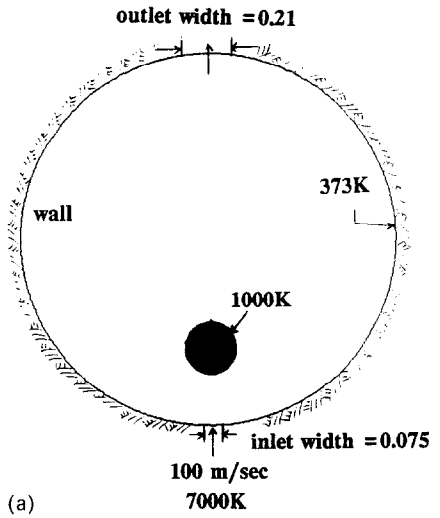

FIG. 1. Schematic illustration of geometries and boundary conditions adopted in the present study. (a) Planar configuration; (b) side view of axisymmetric configuration.

2. FLOW CONFIGURATIONS, PHYSICAL MODELS, AND NUMERICAL METHODS

Schematic illustrations of the geometries and boundary conditions adopted in the present analysis are shown in Fig. 1. For both planar and axisymmetric configurations, a hot plasma jet with uniform temperature and incoming speed of 7000 K and 100 m s^{-1}, respectively, is issued into a large chamber, impinging upon a solid object, then exiting from an outlet on the opposite side from the inlet. In the planar case, both the chamber and the solid object are circular cylinders while in the axisymmetric case, the cylinder is replaced with a solid sphere located in the middle of a circular cylindrical chamber. The object of impingement in both cases is of a constant outside wall temperature of 1000 K and is located directly downstream of, and on-axis with, the jet. The inside wall temperature of the chamber is taken as a constant value of 373 K. A non-uniform grid system of 81 nodes along the streamwise direction and 161 nodes along the cross-stream direction is used for the whole domain within the chamber, and the computation is conducted for half of the domain by enforcing a symmetry condition along the symmetry line of the geometry. A close-up view of the grid distribution surrounding the circular cylinder is given in Fig. 2, which shows that 28 nodes are used to represent the geometry of half of the cylinder (from the front stagnation point, π, to the rear stagnation point, 2π).

With the incoming velocity, density, and viscosity as the reference values, the Reynolds number based on the object diameter is around 2000. However, for conditions commonly observed in RSP, the flow before entering the chamber must be heated by methods such as magnetic induction [4]. Consequently, the flow entering the chamber usually carries turbulent fluctuations that can substantially alter the qualitative characteristics of the RSP operation. The turbulence effect must be accounted for in order to

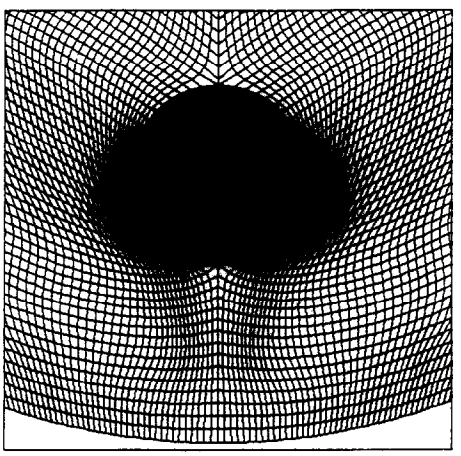

FIG. 2. Close-up view of adaptive grid distribution in region surrounding the circular cylinder of the planar configuration.

yield a physically relevant model for predicting the important process features.

The Favre, i.e. density-weighted, averaged Navier–Stokes equations of mass continuity, momentum, and energy transport, along with a modified k–ε two-equation turbulence closure, are the basis of our computations. The equations are written in generalized coordinates in order to handle both the planar and the axisymmetric problems; they are given in the following with $\alpha = 0$ and 1 designating, respectively, the planar and axisymmetric cases. For the planar case, the independent coordinate, y, should replace r.

2.1. *Continuity*

$$\frac{\partial}{\partial x}(r^\alpha \rho u) + \frac{\partial}{\partial r}(r^\alpha \rho v) = 0 \tag{1}$$

2.2. *u-Momentum (along the axial x-direction)*

$$\frac{1}{r^\alpha}\left[\frac{\partial}{\partial x}(r^\alpha \rho u u) + \frac{\partial}{\partial r}(r^\alpha \rho u v)\right] = -\frac{\partial p}{\partial x} + \frac{1}{r^\alpha}\left[\frac{\partial}{\partial x}\left(r^\alpha \mu_t \frac{\partial u}{\partial x}\right) + \frac{\partial}{\partial r}\left(r^\alpha \mu_t \frac{\partial u}{\partial r}\right)\right] \tag{2}$$

where p is pressure and μ_t is the total viscosity.

2.3. *v-Momentum (along the radial r-direction)*

$$\frac{1}{r^\alpha}\left[\frac{\partial}{\partial x}(r^\alpha \rho u v) + \frac{\partial}{\partial r}(r^\alpha \rho v^2)\right] = -\frac{\partial p}{\partial r} + \frac{1}{r^\alpha}\left[\frac{\partial}{\partial x}\left(r^\alpha \mu_t \frac{\partial v}{\partial x}\right) + \frac{\partial}{\partial r}\left(r^\alpha \mu_t \frac{\partial v}{\partial r}\right)\right] - \frac{2\mu_t v}{r^{2\alpha}} \tag{3}$$

where the last term on the right hand side appears only in the axisymmetric case.

2.4. *Energy equation*

$$\frac{\partial}{\partial x}(r^\alpha \rho u \phi) + \frac{\partial}{\partial r}(r^\alpha \rho v \phi) = \frac{\partial}{\partial x}\left(r^\alpha k_t \frac{\partial T}{\partial x}\right) + \frac{\partial}{\partial r}\left(r^\alpha k_t \frac{\partial T}{\partial r}\right) \tag{4}$$

where ϕ is enthalpy, T is temperature, and k_t is the total thermal conductivity. It is noted that for argon, the radiation heat transfer is negligible compared to other transfer modes if the gas temperature is lower than 9500 K [5]. It is noted that the Mach number of the incoming jet is about 0.3. Furthermore, due to the sudden expansion and rapid cooling of the jet, the Mach number within the whole enclosure is low and the contribution of the kinetic energy to energy balance is insignificant. Since the ratio of the Reynolds number to Mach number is high, the viscous dissipation terms are low, and are neglected as well. Finally, the local thermodynamics equilibrium is assumed throughout and the effect of dissociation and recombination is neglected, which for argon seem to be reasonable working assumptions in view of the rapid cooling rate and low Mach number of the jet.

2.5. *Turbulence closure*

Firstly, the standard forms of the transport equations for the turbulent kinetic energy, k, and the rate of dissipation of turbulent kinetic energy, ε, as given by Launder and Spalding [6], are adopted. The eddy viscosity, μ_t, is determined according to the following formula:

$$\mu_t = \frac{C_\mu \rho k^2}{\varepsilon} + \mu \tag{5}$$

where μ is the molecular viscosity. The original value of the coefficient C_μ proposed by Launder and Spalding was 0.09. Later, in order to accommodate the region of relatively low turbulent Reynolds number, various works suggested that C_μ be modified as

$$C_\mu = 0.09 f_\mu. \tag{6}$$

The function f_μ represents a damping mechanism of the turbulent transport in a region where the turbulent fluctuation is not vigorous. A number of low Reynolds number k–ε models for single-phase flows have been proposed and tested [7–9]. The following formula appears to yield good performance under many conditions:

$$f_\mu = \exp\left[\frac{-3.4}{\left(1 + \frac{R_t}{50}\right)^2}\right] \tag{7}$$

$$R_t = \frac{\rho k^2}{\mu \varepsilon}. \tag{8}$$

The magnitude of f_μ depends on the local turbulent Reynolds number, R_t. The above formula for f_μ was originally proposed by Launder and Sharma [9, 10]. A turbulent Prandtl number of 0.8 is used for all cases studied.

The original as well as the modified k–ε turbulence models were developed in the context of the constant property flows. Extending them to solve the flows with substantial property variations is obviously not straightforward. Some of the modeling related issues between the Reynolds-averaged and the Favre-averaged equations have been discussed by Pope [11]. Experiences gathered in the area of turbulent reactive flow calculations [12, 13] indicate that by resorting to the Favre, instead of the Reynolds, averaging process, the density fluctuation terms do not appear explicitly, and the turbulence closures developed for the variable property flows can often be applied with accuracy comparable to that for the constant property flows. It is with this background that the modified k–ε model outlined above is adopted. In view of the large temperature variations encountered in the present system, the thermodynamic properties cannot be taken as constants. The present model is developed based on the notion of local thermodynamic equilibrium, which

Table 1. Properties of argon gas in MKS units

Temperature (K)	300	600	1400	3000	6000	7000	8000
Density, ρ ($\times 10^2$)	53.4	26.7	11.4	5.34	—	—	2.0
Thermal conductivity, k ($\times 10^2$)	2.42	—	6.50	10.6	17.6	—	35.7
Dynamic viscosity, μ ($\times 10^5$)	3.06	—	8.31	13.6	21.3	—	25.5
Specific heat, C_p ($\times 10^{-2}$)	5.21	—	—	—	—	5.55	6.90

Note: The values shown are used as the reference points. Properties at temperatures other than the above tabulated ones are calculated by linear interpolation.

appears reasonable due to the fact that the Mach number is low throughout because the high speed fluids are also of high temperature. The gas properties are determined by the local gas temperature, as given in Table 1.

The present level of approximations of the governing equations has been adopted for modeling both the turbulent and laminar processes of the high temperature arc and torch flows [4, 5, 14–16] with meaningful results obtained.

The above set of equations is solved using a pressure-correction type of semi-implicit finite volume formulation in arbitrary curvilinear coordinates [17, 18]. The convection terms in the momentum equations are approximated by a second-order upwind scheme. The pressure as well as all the second-order derivative terms are discretized by second-order central difference schemes. An adaptive grid method developed previously [19] is extended and applied here. The method is based on the multiple one-dimensional procedure of equidistribution concept. The weighting function is comprised of the contributions from the smoothness constraint, and combined velocity and temperature gradients. The original method treats the changes of flow variable along each family of coordinates independently. In the present work, the Laplace equation is used as a postprocessor to reduce the mesh skewness. The Laplace equation is solved by a point-SOR procedure. It is well established that the point-SOR method can first eliminate the high wave number parts of error during the course of iteration. It is relatively slow in overall convergence. Hence, by utilizing the procedure, for, say, five to ten iterations, the resulting grid system can exhibit improved control of grid skewness while largely retaining the same clustering characteristics, both desirable for our purpose.

Regarding the question of the grid resolution used in the computation, since there is no available experimental measurement to assess the quantitative accuracy of the solutions, it is our opinion that for problems as complicated as the present one, computation may be best used as a tool to offer some understanding of the major physical characteristics involved. It can also delineate the qualitative trends of the overall process dynamics.

3. RESULTS AND DISCUSSION

The mean flow field for all cases is considered to be stationary in time. For the present flow configuration, depending on the inlet and boundary conditions, the flow can be non-stationary in time. As already mentioned, because the flow has been agitated before entering the chamber, the incoming turbulence level is relatively high. The level of incoming turbulent kinetic energy is considered to be $0.05(u_{\text{inlet}})^2$ or higher. If k_{inlet} is lower than $0.02(u_{\text{inlet}})^2$, the model predicts that the mean flow field becomes non-stationary. For the range of k_{inlet} considered in the present work, converged stationary mean flow solutions can always be obtained.

3.1. *Planar configuration*

The planar configuration, comprising a slot jet interacting with a circular cylinder within a circular cylinder chamber, is investigated first. Two levels of turbulent kinetic energy of the incoming jet, k_{inlet}, are considered; in the first case, $k_{\text{inlet}} = 0.05(u_{\text{inlet}})^2$, while in the second case, $k_{\text{inlet}} = 0.15(u_{\text{inlet}})^2$. The value of the turbulent dissipation rate at the inlet, $\varepsilon_{\text{inlet}}$, is assigned according to the equilibrium condition, i.e.

$$\varepsilon_{\text{inlet}} = \frac{k_{\text{inlet}}^{3/2}}{0.09 L_{\text{inlet}}} \tag{9}$$

where L_{inlet}, the inlet width, is chosen as the length scale. This practice has been commonly adopted for complex flow computations [12, 13].

Based on the solutions obtained on the original curvilinear grid system, a new adaptive grid is generated and the final solution is obtained on it. A close-up view of the adaptive grid distribution in a region surrounding the cylinder for the case of 5% turbulent fluctuation is given in Fig. 2, which depicts clustered and non-uniform grid concentration in the region where the flow accelerates, resulting in higher solution gradients there. In the rear domain of the cylinder, the flow slows down and the velocity as well as the temperature gradient there become more modest. Selected plots of convection, temperature, and turbulence transport characteristics are given in Figs. 3 and 4 for the two different incoming turbulent intensities. Both similarities and differences can be readily observed.

Overall, as expected, with a higher value of k_{inlet}, the turbulent mixing capability is stronger, resulting in faster decay rates of the jet temperature both before and after impinging on the solid cylinder. Accordingly, the solution for a higher k_{inlet} exhibits higher gas temperature levels within the chamber and lower gas temperatures at the chamber exit. A striking difference

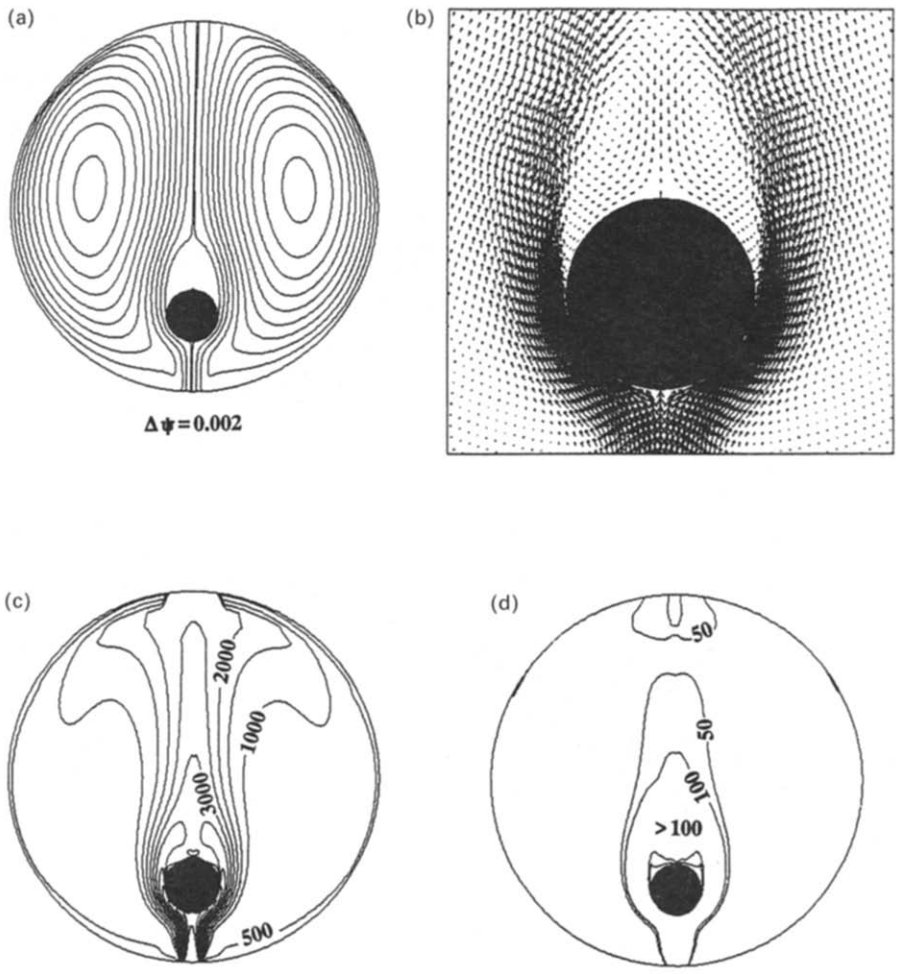

FIG. 3. Solution characteristics of the planar configuration with $k_{inlet} = 0.05(\bar{u}_{inlet})^2$. (a) Streamlines in whole domain, (b) velocity vectors around circular cylinder, (c) isotherm distribution, and (d) turbulent Reynolds number distribution.

exists in the velocity field, where for the case of $k_{inlet} = 0.05(u_{inlet})^2$, there is a massive separation at the rear end of the solid cylinder; for the case of $k_{inlet} = 0.15(u_{inlet})^2$, however, despite the flow also experiencing similar adverse pressure gradients around the solid cylinder, a higher turbulence level causes the separation to be completely suppressed. The mechanism behind this phenomenon is identical to the well-known fact that the viscous drag of the turbulent flow over a circular cylinder is less than that of the laminar flow due to the retardation of the point of flow separation [20, p. 97]. Another noticeable feature of the convection field is the pair of contra-rotating eddies formed within the chamber. The eddies are induced by the combined effects of the high speed jet and the no-slip chamber wall conditions. The overall strengths of these eddies are not much affected by k_{inlet}.

The distribution of the turbulent Reynolds number reveals information that can be utilized to help interpret the aforementioned solution characteristics with more physical insight. As evidenced by the low Reynolds number modification expressed in the form of the function f_μ, the flow is considered to be fully turbulent only when the turbulent Reynolds number is high enough. According to the present turbulence model, a smaller R_t causes a lower f_μ, which, in agreement with reality, reduces μ_t. For example, a value of $R_t = 100$ corresponds to $f_\mu = 0.685$, meaning that the resulting eddy viscosity will be less than 70% of the value yielded by the original k–ε model. Figure 3(d) shows that for the case of $k_{inlet} = 0.05(u_{inlet})^2$, the values of R_t at the rear of the solid cylinder become lower than 50, resulting in a much reduced influence of turbulence on the overall transport processes. Consequently, the flow separates there. For $k_{inlet} = 0.15(u_{inlet})^2$, on the other hand, the level of R_t in the region surrounding the solid cylinder is higher, indicating a stronger ability for the fluid to resist flow separation. It is noted that in the bulk domain occupied by the induced eddies, the turbulent Reynolds number is low for both cases. This observation sug-

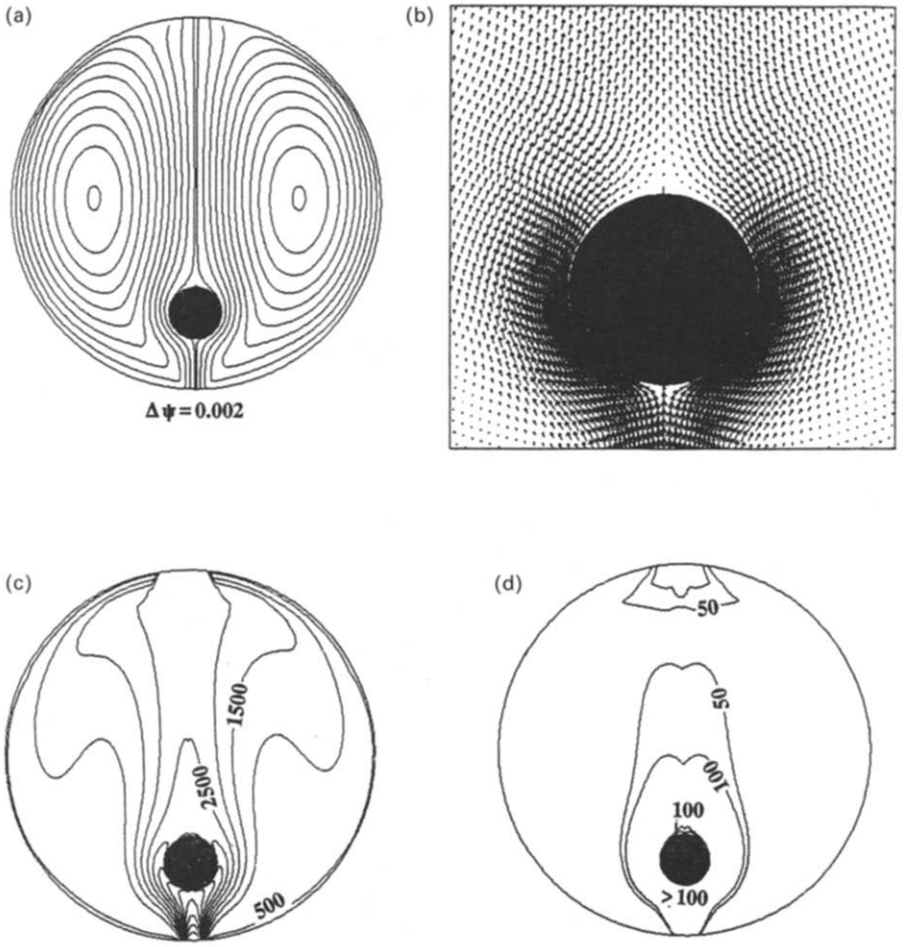

FIG. 4. Solution characteristics of the planar configuration with $k_{inlet} = 0.15(\bar{u}_{inlet})^2$. (a) Streamlines in whole domain, (b) velocity vectors around circular cylinder, (c) isotherm distribution, and (d) turbulent Reynolds number distribution.

gests that the jet-induced eddies are not very turbulent.

Figure 5 depicts more detailed profiles of the important thermal characteristics of the process. The solutions associated with the two values of k_{inlet} are compared. Three quantities are displayed in Fig. 5, including the temperature profile along the symmetry line from the chamber inlet to the outlet, and the effective heat transfer coefficient, h, as well as the Nusselt number, Nu, along the surface of the solid cylinder. The temperature profiles show monotonic, smooth decays from the inlet toward the solid cylinder until the fluid reaches the front stagnation point, where sudden and drastic drops of several thousand Kelvin are observed. At the rear stagnation point, the fluids maintain temperatures of more than 2000 K for both cases; they then gradually decay toward the chamber outlet.

As expected, the jet of higher turbulent fluctuation experiences a higher degree of mixing before reaching the solid cylinder, as indicated by the substantially faster rate of decay of the temperature profile in the region upstream of the solid cylinder. Accordingly, the temperature variation from the fluid to the cylinder wall at the front stagnation point is smaller for the case of $k_{inlet} = 0.15(u_{inlet})^2$; however, this does not mean that its effective heat transfer coefficient h at the front stagnation point is lower. On the contrary, as shown in Fig. 5(b), the value of h for $k_{inlet} = 0.15(u_{inlet})^2$ is more than 2.5 times that for $k_{inlet} = 0.05(u_{inlet})^2$. The difference exhibited between h and T is, of course, caused by the effect of k_{inlet} on the values of eddy thermal conductivity at the front stagnation point. A higher k_{inlet} results in higher turbulence production at the front stagnation point, which, in turn, results in higher μ_t and k_t there.

For flow with $k_{inlet} = 0.15(u_{inlet})^2$, while the temperature at the front stagnation point is lower, it has higher eddy viscosity. Figures 5(a) and (b) together indicate that the ratio of k_t at the front stagnation point between $k_{inlet} = 0.15(u_{inlet})^2$ and $k_{inlet} = 0.05(u_{inlet})^2$ is more than a factor of 3; this ratio

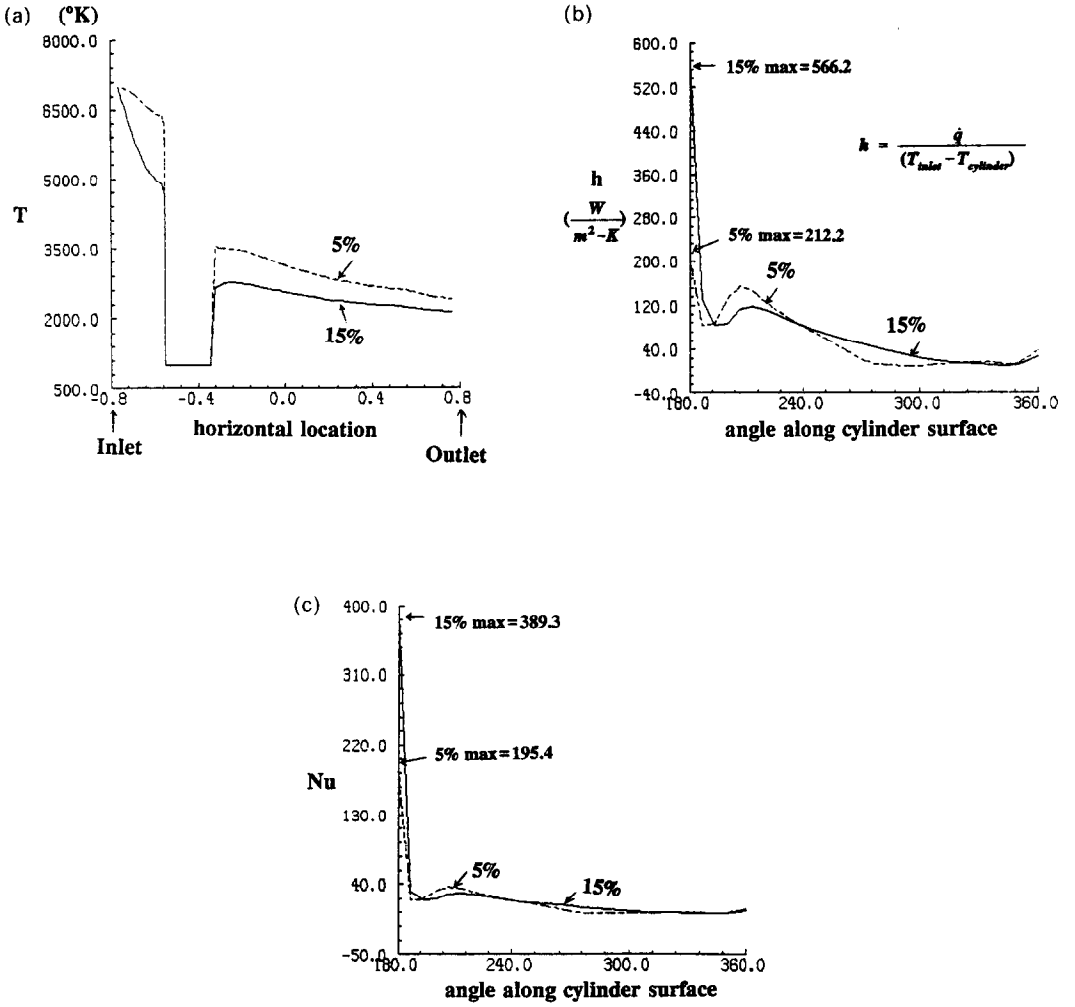

FIG. 5. Effect of k_{inlet} on (a) temperature profile along symmetry line of the domain, (b) heat transfer coefficient, and (c) Nusselt number on the surface of circular cylinder of the planar configuration.

is higher than that of the inlet value between the two cases. Under the equilibrium condition, μ_t (and k_t) is proportional to $(k_{inlet})^{0.5}$. Hence, it is clear that it is the local turbulence production around the front stagnation point instead of the higher turbulence level of the incoming jet itself that is responsible for the enhanced heat transfer rate there. One should note that the definition adopted here for h is based on the temperature difference between the incoming jet and the outside wall of the solid cylinder, i.e.

$$h = \frac{\dot{q}}{T_{inlet} - T_{cylinder}} \tag{10}$$

where $\dot{q}$ is the local heat transfer rate from the fluid to the solid surface. Figure 5(c) compares the Nusselt number, defined as

$$Nu = \frac{hd}{k_l}, \tag{11}$$

where d is the diameter of the solid cylinder and k_l is the molecular thermal conductivity of the fluid. The effect of k_{inlet} on Nu exists mainly in a region which is close to the front stagnation point. Downstream of the stagnation point, Nu appears to be very insensitive to k_{inlet}. The qualitative trends exhibited in Fig. 5 are similar to those reported for the uniform flow over a cylinder [20–22]. The quantitative variations are, of course, different. Regarding the reported studies of the heat transfer enhancement due to turbulence, for a cylinder in crossflow, it has been shown that an increase in the free-stream turbulence intensity from 0 to 3% can yield enhancements in the local heat transfer coefficient by as much as 80% [22, 23]. Similar trends have been confirmed either directly or indirectly for impinging jets [24]. Although the specific conditions such as the temperature and velocity levels and the geometric complexities of the present prob-

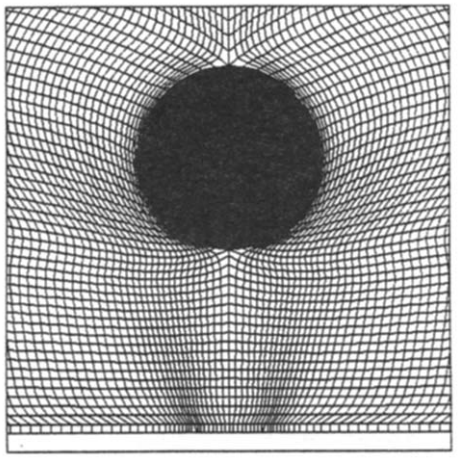

FIG. 6. Close-up view of adaptive grid distribution in region surrounding the sphere of the axisymmetric configuration.

lems are different, the general trends observed here in terms of turbulent heat transfer enhancement are very consistent. Furthermore, the solutions obtained here can link the change in turbulence level to both heat transfer and convection characteristics in an unequivocal manner, yielding some insights of the interaction among different physical mechanisms.

3.2. *Axisymmetric configuration*

Next, the case of a circular jet issued into a cylindrical chamber where a solid sphere is located in the center is studied. A close-up view of the adaptive grid distribution is given in Fig. 6. It is noted that except for the radius effect, all other geometric as well as physical boundary specifications of both the planar and the axisymmetric configurations are the same. The main difference in transport characteristics between the planar and the axisymmetric cases is the

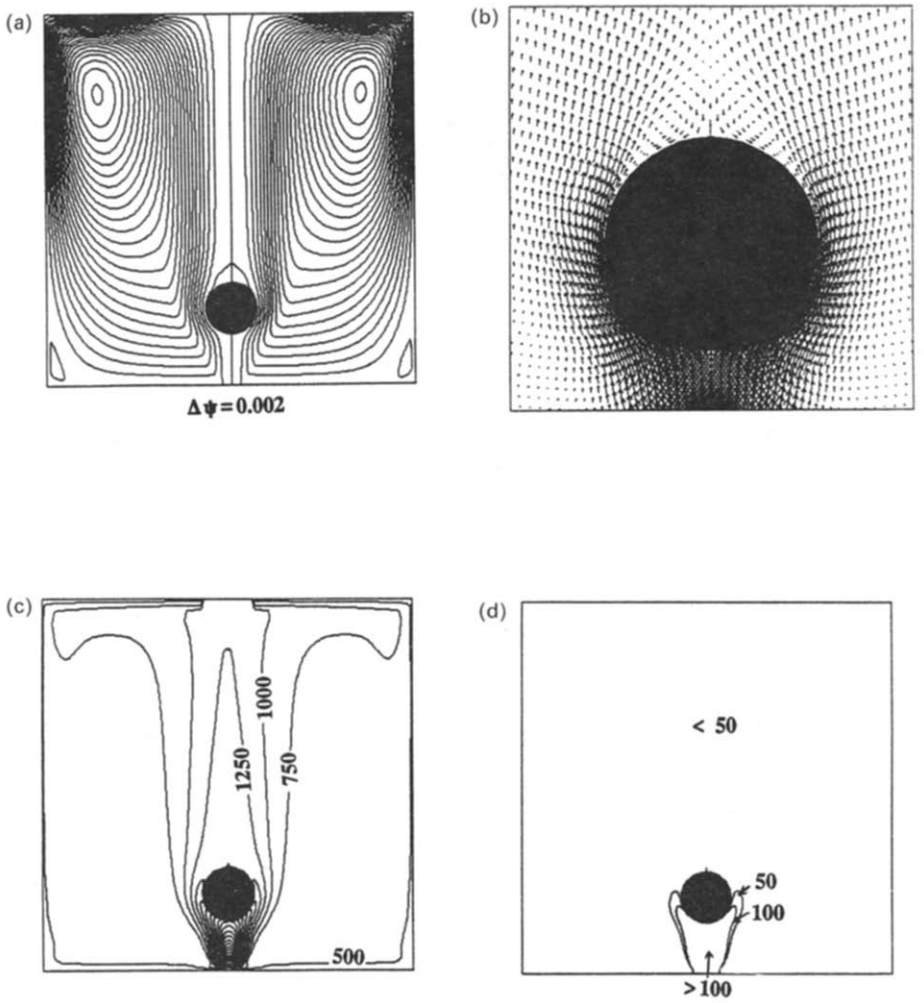

FIG. 7. Solution characteristics of the axisymmetric configuration with $k_{\text{inlet}} = 0.15(\bar{u}_{\text{inlet}})^2$. (a) Streamlines in whole domain, (b) velocity vectors around sphere, (c) isotherm distribution, and (d) turbulent Reynolds number distribution.

area ratio between the jet and the chamber. For the planar case, the slot jet is of the same height as the chamber, and the area ratio is proportional to L_{inlet}/D, where D is the chamber diameter. For the axisymmetric case, the area ratio now becomes $(L_{inlet}/D)^2$. Since the circular jet occupies a far smaller percentage of the overall area in the chamber, the effect of the ambient fluid on the jet flow mixing and entrainment is much higher in the axisymmetric configuration. Accordingly, the rate of drop of the temperature and the rate of decay of the turbulence of the jet are higher in the axisymmetric case.

The solutions of velocity, temperature, and turbulent Reynolds number for $k_{inlet} = 0.15(u_{inlet})^2$ for the axisymmetric configuration are presented in Fig. 7. Compared to the case of planar configuration with the same k_{inlet}, the temperature distribution of the present circular jet decreases faster. In the planar configuration, more vigorous turbulent fluctuation associated with a higher k_{inlet} is responsible for both a faster mixing rate in the temperature field and a stronger resistance to flow separation in the velocity field. Here, the difference in area ratio between the two geometries alters some of the qualitative aspects of the turbulent transport. Since the strength of the turbulence intensity of the circular jet decays much faster than that of the planar jet, the region in which R_t is larger than 100 in the axisymmetric configuration occupies a small domain between the chamber inlet and the solid sphere, while that in the planar configuration occupies a larger region, surrounding the whole solid cylinder. This faster rate of decrease of R_t in the axisymmetric case means that the fluids quickly lose their ability to resist the adverse pressure gradient, and hence, flow separation occurs even with $k_{inlet} = 0.15(u_{inlet})^2$. A case of higher k_{inlet}, $0.25(u_{inlet})^2$, has also been computed with identical geometry and boundary conditions to the previous cases; it is found that flow separation is still unavoidable for the axisymmetric case. Hence, in summary, for the planar

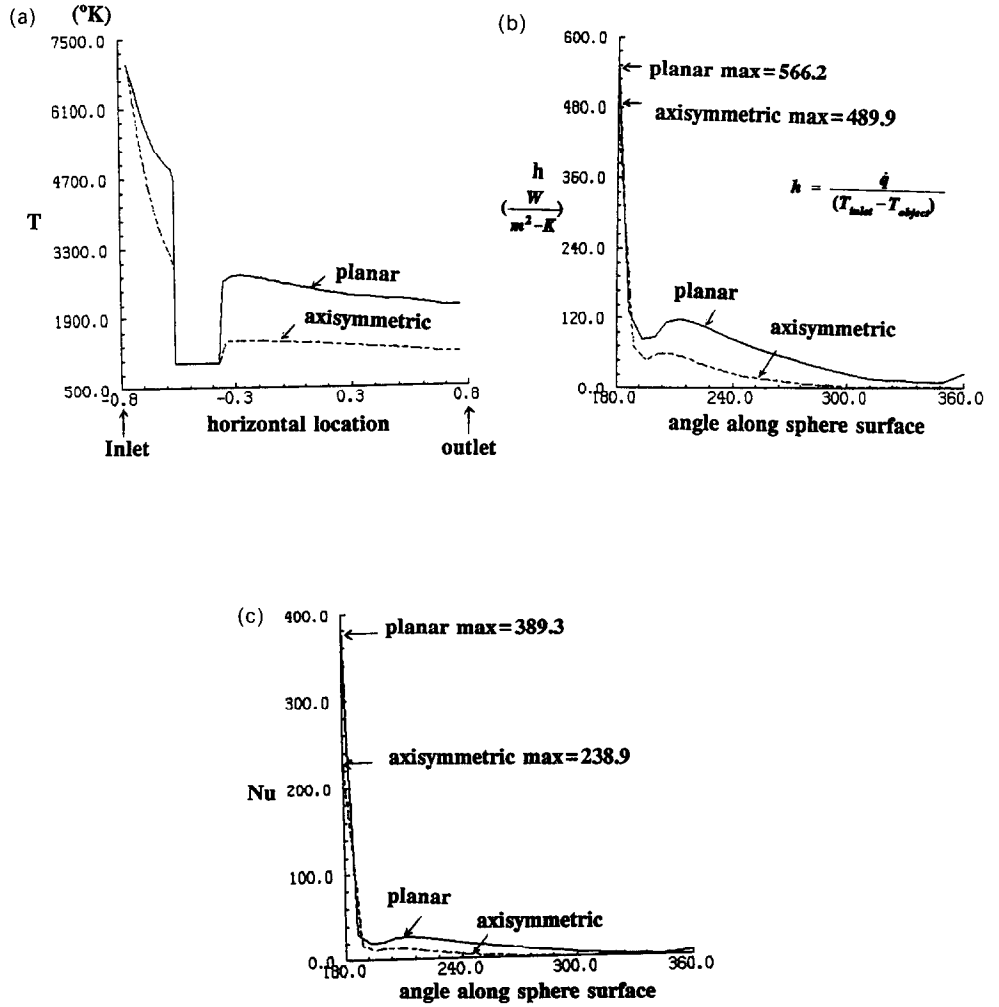

FIG. 8. Comparison of (a) temperature profile along symmetry line of the domain, (b) heat transfer coefficient, and (c) Nusselt number on the object surface between planar and axisymmetric configurations, with $k_{inlet} = 0.15(\bar{u}_{inlet})^2$.

configuration a higher k_{inlet} is effective in enhancing the heat transfer rate and in suppressing the flow separation; for the axisymmetric configuration, it is not able to suppress the flow separation. Furthermore, although for both the planar and the axisymmetric configurations recirculating eddies are induced within the chamber, the difference in the area ratio results in much weaker overall convection strength for the axisymmetric case.

The temperature, heat transfer coefficient, and Nusselt number profiles between the planar and the axisymmetric configurations for the case of $k_{inlet} = 0.15(u_{inlet})^2$ are compared in Fig. 8. Consistent with the argument already made, the levels of temperature, h, and Nu associated with the axisymmetric configuration are lower than those associated with the planar configuration.

4. SUMMARY AND CONCLUSION

The interaction of a superheated turbulent plasma jet and a solid object in terms of heat transfer and convection features is studied in the present work. Both planar and axisymmetric configurations are investigated. A low Reynolds number version of the k–ε two-equation model along with a finite-volume solution technique are utilized in the context of an adaptive non-orthogonal grid system. A strong influence of the inlet turbulence intensity is observed; it is responsible for not only the enhanced effectiveness of the turbulent mixing within the gas phase and the heat transfer between gas and solid, but also the qualitative variations in the convection characteristics. For the planar configuration containing a slot jet, the increased turbulence intensity of the incoming fluid can help resist the adverse pressure gradient and suppress the flow separation. For the axisymmetric configuration containing a circular jet, the much smaller area ratio of the jet compared to the ambient gas volume causes the flow to separate under virtually all practical conditions. Nevertheless, regarding the implications of heat transfer rate in an RSP operation, it appears that the flow separation alone has little effect on the heat transfer distribution. It seems that the differences in turbulence production around the front stagnation point, caused by k_{inlet}, are responsible for the major change in overall heat transfer effectiveness.

REFERENCES

1. S. K. Das, B. H. Kear and C. M. Adam (Editor), *Rapidly Soldified Crystalline Alloys*. The Metallurgical Society, Warrendale, PA (1985).
2. R. Mehrabian, Rapid solidification, *Int. Metals Rev.* **27**, 185–208 (1982).
3. J. Feinman (Editor), *Plasma Technology in Metallurgical Processing*. Iron and Steel Society, Warrandale, PA (1987).
4. D. Y. C. Wei, B. Farouk and D. Apelian, Melting metal powder particles in an inductively coupled R.F. plasma torch, *Metall. Trans. B* **19**, 213–226 (1988).
5. R. J. Miller and J. R. Ayen, Temperature profiles and energy balances for an inductively coupled plasma torch, *J. Appl. Phys.* **40**, 5260–5271 (1969).
6. B. E. Launder and D. B. Spalding, The numerical computation of turbulent flows, *Comput. Meth. Appl. Mech. Engng* **3**, 269–289 (1974).
7. V. C. Patel, W. Rodi and G. Scheuerer, Turbulent models for near-wall and low Reynolds number flows: a review, *AIAA J.* **23**, 1308–1319 (1985).
8. C. K. G. Lam and K. A. Bremhorst, A modified form of the k–ε model for predicting wall turbulence, *ASME J. Fluids Engng* **103**, 1308–1319 (1981).
9. B. E. Launder, On the computation of convective heat transfer in complex turbulent flows, *ASME J. Heat Transfer* **110**, 1112–1128 (1988).
10. B. E. Launder and B. I. Sharma, Application of the energy dissipation model of turbulence to the calculation of flow near a spinning disc, *Lett. Heat Mass Transfer* **1**, 131–138 (1974).
11. S. B. Pope, The statistical theory of turbulent flame, *Phil. Trans. R. Soc. Lond.* **291**, 529–568 (1979).
12. W. P. Jones and J. H. Whitelaw, Modeling and measurements in turbulent combustion, *20th Symp. (Int.) on Combustion*, pp. 233–249. The Combustion Institute, Pittsburgh, PA (1984).
13. W. Shyy, M. E. Braaten and D. L. Burrus, Study of three-dimensional gas-turbine combustor flows, *Int. J. Heat Mass Transfer* **32**, 1155–1164 (1989).
14. J. J. Lowke, Calculated properties of vertical arcs stabilized by natural convection, *J. Appl. Phys.* **50**, 147–157 (1979).
15. D. K. McLain and R. J. Zollweg, Convection in horizontal high-pressure mercury, mercury plus iodine, and metal halide additive arcs, *J. Appl. Phys.* **52**, 199–209 (1981).
16. P. Y. Chang, W. Shyy and J. T. Dakin, A study of three-dimensional natural convection in high-pressure mercury lamps, Parts I and II, *Int. J. Heat Mass Transfer* **33**, 483–493, 495–506 (1990).
17. W. Shyy, S. S. Tong and S. M. Corea, Numerical recirculating flow calculation using a body-fitted coordinate system, *Numer. Heat Transfer* **8**, 99–113 (1985).
18. W. Shyy and T. C. Vu, On the adoption of velocity variable and grid system for fluid flow computation in curvilinear coordinates, *J. Comput. Phys.* **92**, 82–105 (1991).
19. W. Shyy, Computation of complex fluid flows using an adaptive grid method, *Int. J. Numer. Meth. Fluids* **8**, 475–489 (1988).
20. A. Zukauskas, Heat transfer from tubes in crossflow. In *Advances in Heat Transfer* (Edited by J. P. Hartnett and T. F. Irvine, Jr.), Vol. 19, pp. 87–160. Academic Press, New York (1987).
21. E. R. G. Eckert and E. Soehngen, Distribution of heat-transfer coefficients around cylinders in crossflow at Reynolds numbers from 20 to 500, *Trans. ASME* **74**, 343–347 (1952).
22. J. Kestin, The effect of free-stream turbulence on heat transfer rates. In *Advances in Heat Transfer* (Edited by T. F. Irvine and J. P. Hartnett), Vol. 3, pp. 1–32. Academic Press, New York (1966).
23. G. W. Lowery and R. I. Vachon, The effect of turbulence on heat transfer from heated cylinders, *Int. J. Heat Mass Transfer* **18**, 1229–1242 (1975).
24. R. Gardon and J. C. Akfirat, The role of turbulence in determining the heat-transfer characteristics of impinging jets, *Int. J. Heat Mass Transfer* **8**, 1261–1272 (1965).

CARACTERISTIQUES DE TRANSFERT THERMIQUE ET DE CONVECTION D'UN JET TURBULENT SURCHAUFFE EN INTERACTION AVEC UN OBJET SOLIDE

Résumé—On étudie numériquement les caractéristiques associées de la convection et du transfert de chaleur dans l'interaction entre un jet turbulent surchauffé d'argon et un objet solide, un sujet d'importance critique pour les mécanismes rapides de solidification. Duex configurations sont simulées, un cas planaire qui inclut un jet plat dans une chambre cylindrique circulaire et frappant un cylindre solide, et un cas axisymétrique de jet circulaire dans une chambre circulaire cylindrique et frappant une sphère solide. On étudie les effets de l'intensité de turbulence du jet sur les caractéristiques de la convection et du transfert thermique; dans les deux configurations le transfert turbulent peut améliorer le transfert thermique en créant des distributions fortement non uniforme autour de l'objet. A cause des différences entre les deux géométries, la séparation de l'écoulement peut être complètement supprimée par une intensité de turbulence élevée dans la configuration planaire mais pas dans l'autre axisymétrique. On essaie d'interpréter et d'éclaircir les différentes caractéristiques obtenues dans les solutions et de gagner une compréhension physique des conditions d'apparition des mécanismes.

WÄRMEÜBERGANG UND KONVEKTION BEI DER WECHSELWIRKUNG ZWISCHEN EINEM ÜBERHITZTEN TURBULENTEN STRAHL UND EINEM FESTKÖRPER

Zusammenfassung—In der vorliegenden Arbeit werden der Wärmeübergang und die damit verbundene Konvektion, die bei einer Wechselwirkung zwischen einem überhitzten turbulenten Argonstrahl und einem Festkörper auftreten, numerisch untersucht. Dieses Problem ist von sehr großer Wichtigkeit bei modernen Prozessen einer schnellen Verfestigung. Es werden zwei Strömungskonfigurationen simuliert, eine ebene Anordnung, bei der ein schlitzförmiger Strahl in eine kreisförmig-zylindrische Kammer eingebracht und durch einen festen Zylinder beeinflußt wird, und eine weitere, achsensymmetrische Anordnung, bei der ein kreisförmiger Strahl in eine kreisförmige zylindrische Kammer eingebracht und von einer festen Kugel beeinflußt wird. Es werden die Einflüsse der Turbulenzintensität des eintretenden Strahls auf Konvektion und Wärmeübergang untersucht. Bei beiden Anordnungen kann der turbulente Transport dazu beitragen, den Wärmestrom durch stark ungleichförmige Verteilungen der Nusselt-Zahl zu erhöhen. Des weiteren kann aufgrund der unterschiedlichen Geometrie die Strömungsseparation bei hoher Turbulenzintensität im Fall der ebenen Anordnung vollständig unterdrückt werden. Dies gelingt bei achsensymmetrischer Anordnung nicht. Es wird versucht, die Eigenheiten, die sich bei der Lösung ergeben, zu interpretieren und zu erklären und so physikalische Einsicht in die zugrundeliegenden Vorgänge zu erhalten.

ХАРАКТЕРИСТИКИ ТЕПЛОПЕРЕНОСА И КОНВЕКЦИИ ПРИ ВЗАИМОДЕЙСТВИИ ПЕРЕГРЕТОЙ ТУРБУЛЕНТНОЙ СТРУИ С ТВЕРДЫМ ТЕЛОМ

Аннотация—Численно исследуются характеристики теплопереноса и связанной с ним конвекции при взаимодействии между перегретой турбулентной струей аргона и твердым телом, представляющие исключительную важность в процессах быстрого затвердевания. Моделируются две конфигурации течения: одна является плоской и включает плоскую струю, истекающую в круговую цилиндрическую камеру и набегающую на сплошной цилиндр, другая—осесимметричная, когда круглая струя, истекающая в круговую цилиндрическую камеру, набегает на сплошную сферу. Исследуется влияние интенсивности турбулентности набегающей струи на характеристики конвекции и теплопереноса; при обеих конфигурациях турбулентный перенос может способствовать интенсификации теплопереноса, что приводит к существенно неоднородному распределению чисел Нусселта вокруг твердого тела. Кроме того, за счет различий, обусловленных разной геометрией, отрыв потока может полностью подавляться высокой интенсивностью турбулентности при плоской конфигурации, в отличие от случая осесимметричной конфигурации. Делаются попытки объяснения различных характеристик полученных решений, а также физической интерпретации соответствующих режимов обработки.